Supporting information

Boosting visible-light hydrogen evolution via d-band center engineering in FeP/Graphdiyne heterointerface

Nini Zhao[a,b,c], Jingzhi Wang[a,b,c], Zhengyu Zhou[a,b,c], Miao Wang[a,b,c], Kai Wang[a,b,c]*, Zhiliang Jin[a,b,c]

a. School of Chemistry and Chemical Engineering, North Minzu University, Yinchuan 750021, P.R.China

b. Ningxia Key Laboratory of Solar Chemical Conversion Technology; North Minzu University, Yinchuan 750021, P.R.China

c. Key Laboratory for Chemical Engineering and Technology, State Ethnic Affairs Commission, North Minzu University, Yinchuan 750021, P.R.China

*Corresponding author: Kai Wang

Email: kaiwang@nun.edu.cn

EXPERIMENTAL SECTIONS

Catalysts Characterization

Field emission electron microscopy (FESEM, Zeiss evo 10) and transmission electron microscopy (TEM, Talos F200x) were used to analyze the microstructure of the samples. Fourier transform infrared spectroscopy (FTIR, FTIR-650) was used to analyze the functional group structure of the sample. Raman spectroscopy (LabRAM HR Evolution) was used to study the molecular structure of the sample. Cu Kα radiation X-ray diffraction (XRD, Rigaku INTT-2000) was used to characterize the phase and crystal structure of the sample. Using $BaSO_4$ as the standard, the ultraviolet-visible spectrophotometer (UV-vis DRS, UV-2550) was used to test the light absorption capacity of the sample. The ASAP 2460M nitrogen adsorption instrument was used to perform the nitrogen adsorption-desorption isotherm at 77 K, and the specific surface area and pore volume of the sample were calculated by the Brunauer-Emmett-Teller method, and the pore size distribution of the sample was determined by the Barrett-Joyner-Halenda method. Steady-state and transient fluorescence spectra of samples at room temperature were recorded by FLUOROMAX-4 fluorescence spectrometer. The chemical composition of the samples was evaluated by X-ray photoelectron spectroscopy (XPS, ESCALAB Xi+). An electrochemical workstation (VersaStat4-400) was used to analyze the photoelectrochemical properties of the samples. In a three-electrode system, the platinum sheet is the counter electrode, the calomel electrode is the reference electrode, and the FTO conductive glass is the working electrode. A 300W xenon lamp was used as the light source, the electrolyte was 0.2 M Na_2SO_4 solution, and the immersion area of the working electrode was 1 cm^2.

Photocatalytic hydrogen evolution experiments

The reaction system of the photocatalytic hydrogen production experiment was composed of 9 channels and 5W LED ($\lambda \geq 420$ nm), and the photocatalytic hydrogen evolution experiment was carried out in a closed quartz hydrogen production bottle (62 mL) with TEOA (pH = 9) as the sacrificial reagent and eosin-Y (EY) as the photosensitizer. 5 mg photocatalysts and 10 mg EY were added to the quartz hydrogen

production bottle, 30 mL TEOA solution and magneton were added, ultrasonic, mixed, and nitrogen gas was passed through for 3 min to remove the air in the hydrogen production cylinder, and the hydrogen production cylinder was placed in the reaction system after ultrasonication. After irradiation for 1 h, 0.5 mL of hydrogen was extracted from a gas chromatograph (Tianmei GC7900, TCD, 13X column, N_2 as the carrier), and the above steps were repeated for 1 h for a total of 5 h. The production of hydrogen is measured using an external standard method.

DFT calculations

All theoretical calculations were performed using the CASTEP module within Materials Studio, based on Density Functional Theory (DFT). The generalized gradient approximation of the Perdew-Burke-Ernzerh (GGA-PBE) function governs all theoretical calculations related to exchange interactions. In addition, a 5 × 5 × 4 K-point grid was used for reciprocal space and electronic structure analyses. The parameter was set to 0.01 eV. Specifically, 1.0×10^{-5} Ha, 3.0×10^{-2} eV/Å and 1.0×10^{-3} Å represent the SCF tolerance, maximum allowable force and displacement respectively. Allowing for atomic relaxation results in more accurate theoretical calculations. An energy threshold of 500.00 eV was set as the cut-off energy and the ultra-soft pseudopotential model was used. DFT simulations were performed based on TEM characterization, using FeP (102) and GDY (002) crystal planes for lattice exposure ratio calculations. The Grimme correction (DFT+D3) was utilised for van der Waals (vdW) interactions between the intermediates and catalysts. The energy cut-off was set at 520 eV for the plane-wave basis set and spin effects were also taken into account. The fully relaxed of the structure was considered, with the minimum atomic force set to 0.02 eV/$Å^{-1}$ and 10^{-5} eV set as the energy convergence standard. Following convergence testing, all considered structures were employed, with a Gamma-centered k-point mesh utilising the Monkhorst-Pack method of 5×5×1 to ensure the accuracy and efficiency of the calculations. The surface (basal plane) was modeled by a 2×2 supercell. The strong Coulombic force between transition metal atoms was approximated using DFT+U. The calculated U values of Fe were found to be 3 eV [S1].

Kelvin probe force microscopy (KPFM) measurement

KPFM is a derivative imaging mode of atomic force scanning probe microscopy. It can measure the work function of the material surface and the corresponding morphology. FeP and GDY were dispersed on a conductive substrate (FTO) to prepare the sample. The measurement by KPFM is the potential difference that makes the work function equal between the conductive tip and the sample surface. Therefore, the measured contact potential difference (ΔΦ CPD) is related to the work function of the sample as follows:

$$WF\ (sample) = WF\ (tip) + e \cdot \Delta\Phi\ CPD\ (sample)$$

WF (sample) and WF (tip) are the work functions of the tip and sample respectively and e is the charge constant. ΔΦ CPD (sample) is the contact potential difference between sample and tip.

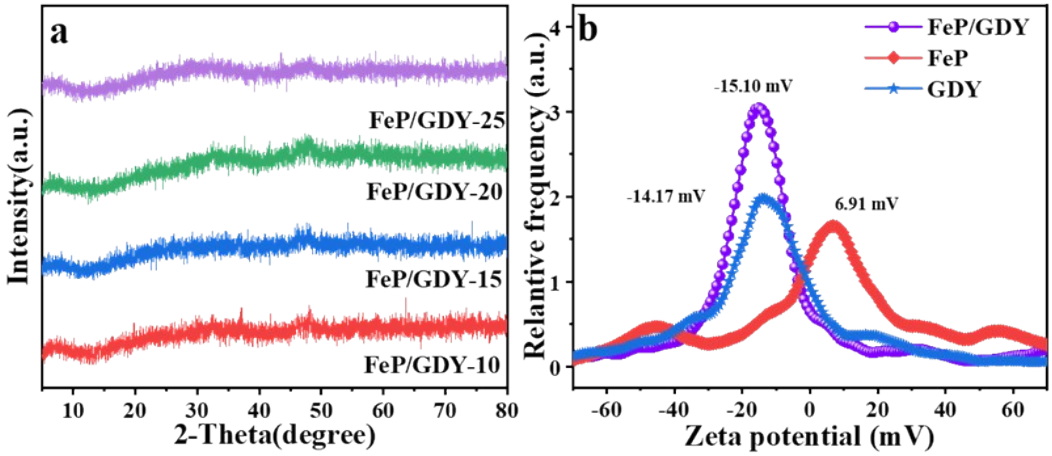

Figure S1. (a) XRD spectra of FeP/GDY-n (n=5, 10, 15, 20, 25); (b) Zeta potentials of FeP, GDY, and FeP/GDY

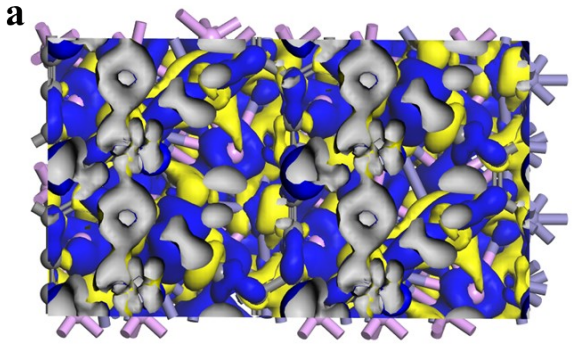

Figure S2. (a) Top view of differential charge density distribution of FeP/GDY (blue area represents charge depletion region, yellow area represents charge accumulation region)

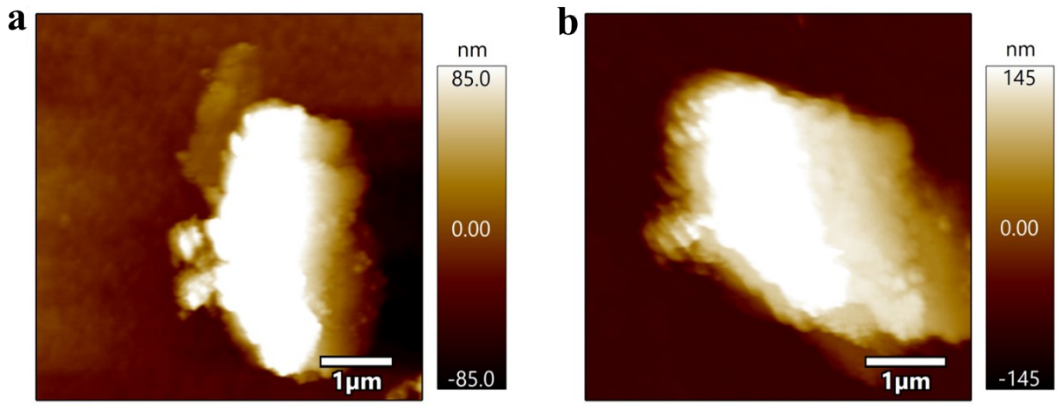

Figure S3. Atomic force microscopy image of (a) FeP and (b) GDY

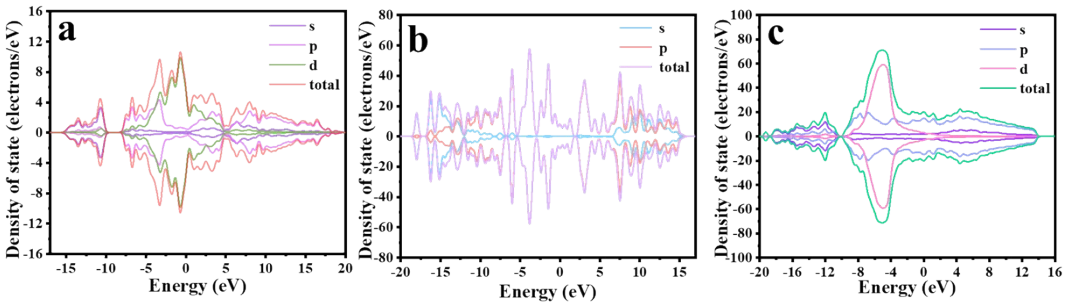

Figure S4. The density of states of (a) FeP, (b) GDY, and (c) FeP/GDY

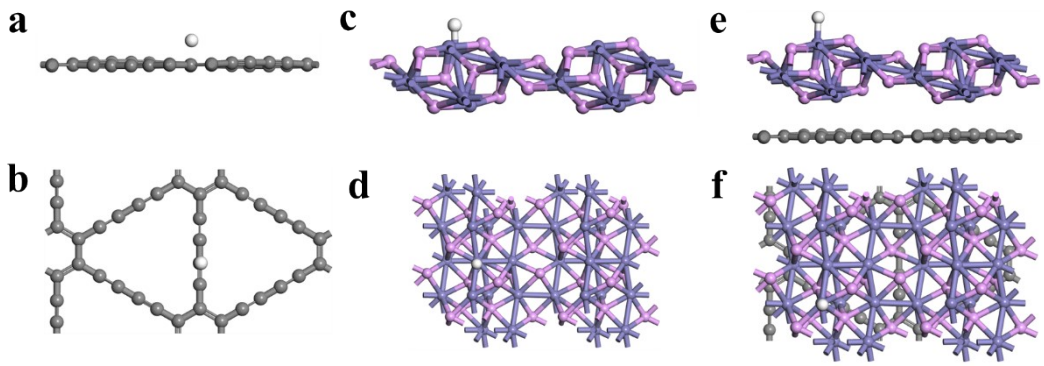

Figure S5. Side view of hydrogen adsorption sites for (a) GDY (c) FeP and (e) FeP/GDY; Top view of hydrogen adsorption sites for (b) GDY (d) FeP and (f) FeP/GDY

Table S1. Specific surface area (S_{BET}), pore volume (D_P), and average pore size distribution (V_P) of FeP, GDY, and FeP/GDY

Samples	S_{BET} ($m^2 \cdot g^{-1}$)	Pore volume ($cm^3 \cdot g^{-1}$)	Average pore size (nm)
FeP	18.39	0.08	17.93
GDY	75.07	0.16	9.05
FeP/GDY	40.36	0.13	13.19

Table S2 comparison of the hydrogen production performance of the same type of photocatalysts

Photocatalyst	Light Source	Sacrificial agents	Production rate	Refs
FeP/GDY	5 W LED	TEOA	3400.26 μmol·g^{-1}·h^{-1}	This
FeP/Cu_3P/$ZnIn_2S_4$	300 W Xenon lamp	Na_2S/Na_2SO_3	142.62 μmol·h^{-1}	[S2]
Mo-CoP@g-C_3N_4	300 W Xenon lamp	TEOA	1470 μmol·g^{-1}·h^{-1}	[S3]
CoP-C/g-C_3N_4	300 W Xenon lamp	TEOA	1503 μmol·g^{-1}·h^{-1}	[S4]
CdS/NiP@UiO-66-NH	300 W Xenon lamp	Na_2S/Na_2SO_3	2103 μmol·g^{-1}·h^{-1}	[S5]
GDY@C_3N_4/Pt	100 W solar simulator	TEOA	798 μmol·g^{-1}·h^{-1}	[S6]

Table S3 Transient attenuation fitting parameters of EY, FeP, GDY and FeP/GDY

Samples	Pre-exponential factors A	Lifetime, <τ>(ns)	Average lifetime <τ>(ns)	χ^2
EY	A_1=100.00	τ_1=0.5164	0.5164	2.61
FeP	A_1=6.79 A_2=93.21	τ_1=5.6494 τ_2=0.4278	0.4564	1.09
GDY	A_1=93.68 A_2=6.02	τ_1=0.3362 τ_2=3.7865	0.3557	1.16
FeP/GDY	A_1=99.82 A_2=0.18	τ_1=0.0063 τ_2=0.5869	0.0063	1.77

REFERENCE

[S1] N. Pinney, J. Kubicki, D. S. Middlemiss, C. Grey, D. Morgan, *Chem. Mater.*, 2009, **21,** 5727-5742.

[S2] H. Qian, X. Lu, J. Wu, X. Fan, S. Xie, X. Xiong, J. Zou, *Int. J. Hydrogen Energy*, 2024, **93,** 1-12.

[S3] Y. Sun, X. Liu, X. Zhao, X. Wang, H. Mu, F, Li, *J. Mater. Chem. A*, 2024, **12,** 28817-28829.

[S4] Z. Huang, X. Long, M. Liu, X. Li, Y. Du, Q. Liu, Y. Chen, S. Guo, R. Chen, *J. Colloid Interface Sci.*, 2024, **653,** 1293-1303.

[S5] Y. Bi, X. Wang, K. Li, C. Wang, Y. Zhang, Q. Liu, *Colloids Surf. A Physicochem. Eng. Aspects*, 2024, **702,** 134929.

[S6] C. Wang, X. Han, Q. Xu, Y. Sun, J. A, M. N. G, J. Li, *J. Mater. Chem. A*, 2023, **11,** 3380-3387.